4. PRODUCTION AND PROPERTIES OF RADIATIONS

$$(\omega_s)_l = \frac{\omega_p}{[(2l+1)/l]^{1/2}} \qquad (4.3.4.34a)$$

(metal sphere in vacuum – the modes are now quantified following the l quantum number in spherical geometry);

$$(\omega_s)_l = \frac{\omega_p}{[(2l+1)/(l+1)]^{1/2}} \qquad (4.3.4.34b)$$

(spherical void within metal).

Thin-film geometry:

$$(\omega_s)^{\pm} = \omega_p \left[\frac{1 \pm \exp(-qt)}{1 + \varepsilon_d} \right]^{1/2} \qquad (4.3.4.35)$$

(metal layer of thickness t embedded in dielectric films of constant ε_d). The two solutions result from the coupling of the oscillations on the two surfaces, the electric field being symmetric for the $(\omega_s)^-$ mode and antisymmetric for the $(\omega_s)^+$.

In a real solid, the surface plasmon modes are determined by the roots of the equation $\varepsilon(\omega_s) = -1$ for vacuum coating [or $\varepsilon(\omega_s) = -\varepsilon_d$ for dielectric coating].

The probability of surface-loss excitation P_s is mostly governed by the $\text{Im}\{-1/[1 + \varepsilon(\omega)]\}$ energy-loss function, which is analogous for surface modes to the bulk $\text{Im}\{-1/[\varepsilon(\omega)]\}$ energy-loss function. In normal incidence, the differential scattering cross section $\mathrm{d}P_s/\mathrm{d}\Omega$ is zero in the forward direction, reaches a maximum for $\theta = \pm\theta_E/3^{1/2}$, and decreases as θ^{-3} at large angles. In non-normal incidence, the angular distribution is asymmetrical, goes through a zero value for momentum transfer $\hbar\mathbf{q}$ in a direction perpendicular to the interface, and the total probability increases as

$$P_s(\varphi) = \frac{P_s(O)}{\cos\varphi}, \qquad (4.3.4.36)$$

where φ is the incidence angle between the primary beam and the normal to the surface. As a consequence, the probability of producing one (and several) surface losses increases rapidly for grazing incidences.

4.3.4.4. *Excitation spectrum of core electrons*

4.3.4.4.1. *Definition and classification of core edges*

As for any core-electron spectroscopy, EELS spectroscopy at higher energy losses mostly deals with the excitation of well defined atomic electrons. When considering solid specimens, both initial and final states in the transition are actually eigenstates in the solid state. However, the initial wavefunction can be considered as purely atomic for core excitations. As a first consequence, one can classify these transitions as a function of the parameters of atomic physics: Z is the atomic number of the element; n, l, and $j = l + s$ are the quantum numbers describing the subshells from which the electron has been excited. The spectroscopy notation used is shown in Fig. 4.3.4.21. The list of major transitions is displayed as a function of Z and E_c in Fig. 4.3.4.22.
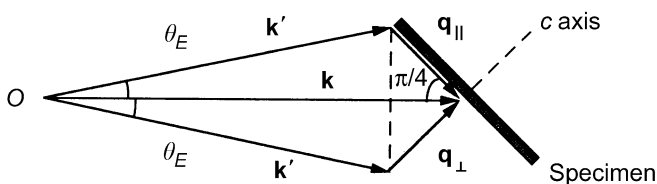
Core excitations appear as edges superimposed, from the threshold energy E_c upwards, above a regularly decreasing background. As explained below, the basic matrix element governing the probability of transition is similar for optical absorption spectroscopy and for small-angle-scattering EELS spectroscopy. Consequently, selection rules for dipole transitions define the dominant transitions to be observed, *i.e.*

$$l' - l = \Delta l = \pm 1 \quad \text{and} \quad j' - j = \Delta j = 0, \pm 1. \qquad (4.3.4.37)$$

This major rule has important consequences for the edge shapes to be observed: approximate behaviours are also shown in Fig. 4.3.4.22. A very useful library of core edges can be found in the EELS atlas (Ahn & Krivanek, 1982), from which we have selected the family of edges gathered in Fig. 4.3.4.23. They display the following typical profiles:

(i) *K edges for low-Z elements* ($3 \le Z \le 14$). The carbon K edge occurring at 284 eV is a nice example with a clear hydrogenic or saw-tooth profile and fine structures on threshold depending on the local environment (amorphous, graphite, diamond, organic molecules, ...); see Isaacson (1972a,b).

(ii) *$L_{2,3}$ edges for medium-Z elements* ($11 \lesssim Z \lesssim 45$). The $L_{2,3}$ edges exhibit different shapes when the outer occupied shell changes in nature: a delayed profile is observed as long as the first vacant d states are located, along the energy scale, rather above the Fermi level (sulfur case). When these d states coincide with the first accessible levels, sharp peaks, generally known as 'white lines', appear at threshold (this is the case for transition elements with the Fermi level inside the d band). These lines are generally split by the spin-orbit term on the initial level into $2p^{3/2}$ and $2p^{1/2}$ (or L_3 and L_2) terms. For higher-Z elements, the bound d levels are fully occupied, and
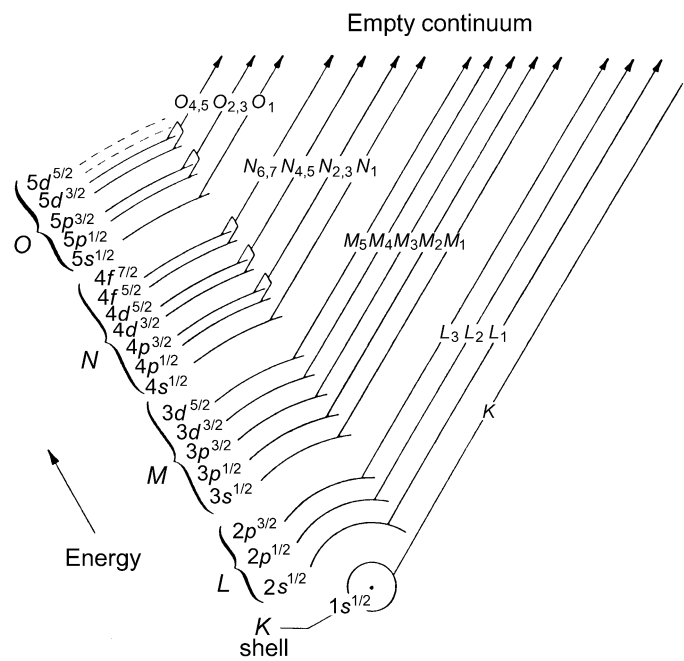
Fig. 4.3.4.20. Geometric conditions for investigating the anisotropic energy-loss function.
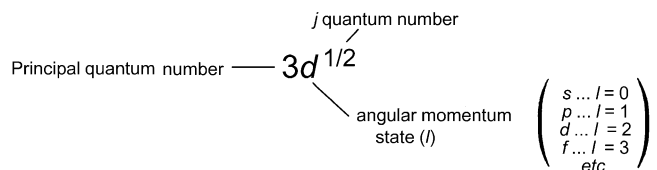
Fig. 4.3.4.21. Definition of electron shells and transitions involved in core-loss spectroscopy [from Ahn & Krivanek (1982)].

no longer contribute as host orbitals for the excited $2p$ electrons. One finds again a more traditional hydrogenic profile (such as for the germanium case).

(iii) $M_{4,5}$ *edges for heavier-Z elements* $(37 \lesssim Z \lesssim 83)$. A sequence of $M_{4,5}$ edge profiles, rather similar to $L_{2,3}$ edges, is observed, the difference being that one then investigates the density of the final f states. White lines can also be detected when the f levels lie in the neighbourhood of the Fermi level, *e.g.* for rare-earth elements.

The deeper accessible signals, for incident electrons in the range of 100–400 kV primary voltage, lie between 2500 and 3000 eV, which corresponds roughly to the middle of the second row of transition elements (Mo–Ru) for the $L_{2,3}$ edge and to the very heavy metals (Pb–Bi) for the $M_{4,5}$ edge.

(iv) A final example in Fig. 4.3.4.23 concerns one of these resonant peaks associated with the excitation of levels just below the conduction band. These are features with high intensity of the same order or even superior to that of plasmons of conduction
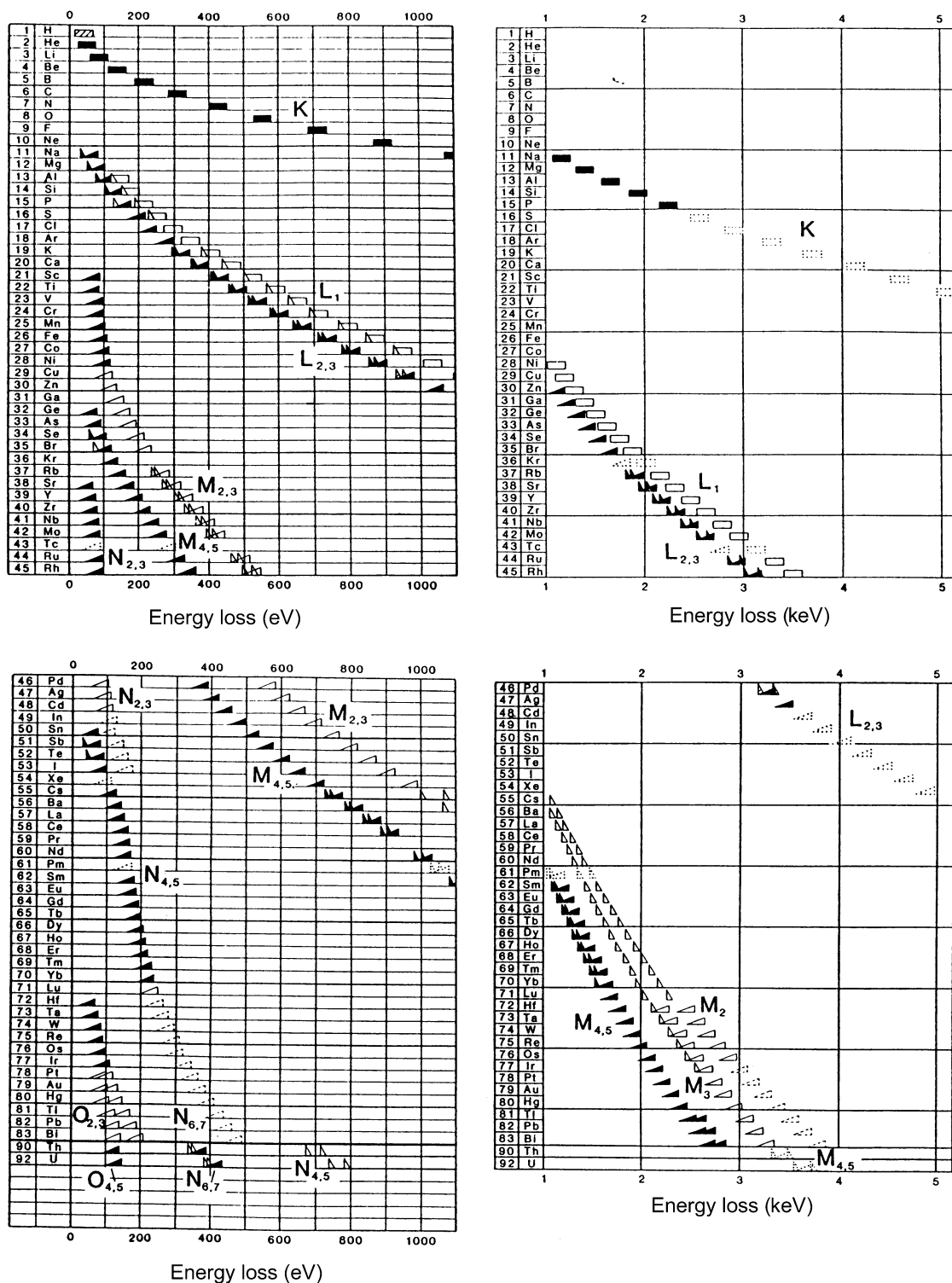

Fig. 4.3.4.22. Chart of edges encountered in the 50 eV up to 3 keV energy-loss range with symbols identifying the types of shapes [see Ahn & Krivanek (1982) for further comments].

band electrons previously described in Subsection 4.3.4.3. It occurs with the $M_{2,3}$ level for the first transition series, with the $N_{2,3}$ level for the second series (for example, strontium in Fig. 4.3.4.23) or with the $O_{2,3}$ level for the third series, including the rare-earth elements. The shape varies gradually from a plasmon-like peak with a short lifetime to an asymmetric Fano-type profile, a consequence of the coupling between discrete and continuum final states of the same energy (Fano, 1961).

4.3.4.4.2. *Bethe theory for inelastic scattering by an isolated atom (Bethe, 1930; Inokuti, 1971, 1979)*

As a consequence of the atomic nature of the excited wavefunction in core-loss spectroscopy, the first step involves deriving a useful theoretical expression for inelastic scattering by an isolated atom. The differential cross section for an electron of wavevector $\mathbf{k}$ to be scattered into a final plane wave of vector $\mathbf{k}'$, while promoting one atomic electron from ψ_0 to ψ_n, is given in a one-electron excitation description by

$$\frac{\mathrm{d}\sigma_n}{\mathrm{d}\Omega\,\mathrm{d}(\Delta E)} = \left(\frac{m_0}{2\pi\hbar^2}\right)^2 \frac{k'}{k} |\langle\psi_n\mathbf{k}'|V(\mathbf{r})|\psi_0\mathbf{k}\rangle|^2; \quad (4.3.4.38)$$
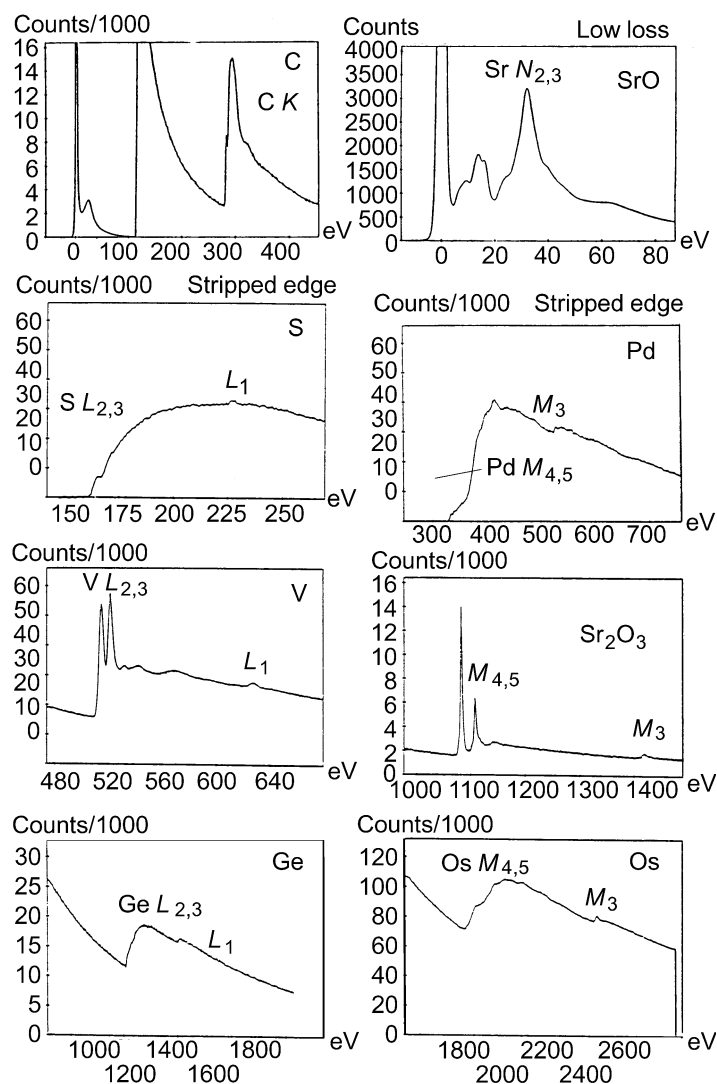

Fig. 4.3.4.23. A selection of typical profiles (K, $L_{2,3}$, $M_{4,5}$, and $N_{2,3}$) illustrating the most important behaviours encountered on major edges through the Periodic Table. A few edges are displayed prior to and others after background stripping. [Data extracted from Ahn & Krivanek (1982).]

see, for instance, Landau & Lifchitz (1966) and Mott & Massey (1952). The potential $V(\mathbf{r})$ corresponds to the Coulomb interaction with all charges (both in the nucleus and in the electron cloud) of the atom. The momentum change in the scattering event is $\hbar\mathbf{q} = \hbar(\mathbf{k} - \mathbf{k}')$. The final-state wavefunction is normalized per unit energy range. The orthogonality between initial- and final-state wavefunctions restricts the inelastic scattering to the only interactions with atomic electrons:

$$\frac{\mathrm{d}\sigma_n}{\mathrm{d}\Omega\,\mathrm{d}(\Delta E)} = \frac{4\gamma^2}{a_0^2 q^4} \frac{k'}{k} |\mathscr{E}_n(\mathbf{q}, \Delta E)|^2. \quad (4.3.4.39)$$

The first part of the above expression has the form of Rutherford scattering. γ is introduced to deal, to a first approximation, with relativistic effects. The ratio k'/k is generally assumed to be equal to unity. This kinematic scattering factor is modified by the second term, or matrix element, which describes the response of the atomic electrons:

$$\mathscr{E}_n(\mathbf{q}, \Delta E) = \left\langle\psi_n\left|\sum_j \exp\left(i\mathbf{q}\cdot\mathbf{r}_j\right)\right|\psi_0\right\rangle, \quad (4.3.4.40)$$

where the sum extends over all atomic electrons at positions $\mathbf{r}_j$. The dimensionless quantity is known as the *inelastic form factor*.

For a more direct comparison with photoabsorption measurements, one introduces the generalized oscillator strength (GOS) as

$$\frac{\mathrm{d}f(\mathbf{q}, \Delta E)}{\mathrm{d}(\Delta E)} = \frac{\Delta E}{R} \frac{|\mathscr{E}_n(\mathbf{q}, \Delta E)|^2}{(qa_0)^2} \quad (4.3.4.41)$$

for transitions towards final states ψ_ε in the continuum [ΔE is then the energy difference between the core level and the final state of kinetic energy ε above the Fermi level, scaled in energy to the Rydberg energy (R)]. Also,

$$f_n(\mathbf{q}) = \frac{E_n}{R} \frac{|\mathscr{E}_n(\mathbf{q})|^2}{(qa_0)^2} \quad (4.3.4.42)$$

for transition towards bound states. In this case, E_n is the energy difference between the two states involved.

The generalized oscillator strength is a function of both the energy ΔE and the momentum $\hbar\mathbf{q}$ transferred to the atom. It is displayed as a three-dimensional surface known as the Bethe surface (Fig. 4.3.4.24), which embodies all information concerning the inelastic scattering of charged particles by atoms. The angular dependence of the cross section is proportional to

$$\frac{1}{q^2} \frac{\mathrm{d}f(\mathbf{q}, \Delta E)}{\mathrm{d}(\Delta E)}$$

at a given energy loss ΔE.

In the small-angle limit ($qr_c \ll 1$, where r_c is the average radius of the initial orbital), the GOS reduces to the optical oscillator strength

$$\frac{\mathrm{d}f(\mathbf{q}, \Delta E)}{\mathrm{d}(\Delta E)} \rightarrow \frac{\mathrm{d}f(0, \Delta E)}{\mathrm{d}(\Delta E)}$$

and

$$\mathscr{E}_n(\mathbf{q}, \Delta E) \rightarrow \mathscr{E}_n(0, \Delta E) = q^2 \left|\left\langle\psi_n\left|\sum_j \mathbf{u}\cdot\mathbf{r}_j\right|\psi_0\right\rangle\right|^2, \quad (4.3.4.43)$$

where $\mathbf{u}$ is the unit vector in the $\mathbf{q}$ direction. When one is concerned with a given orbital excitation, the sum over $\mathbf{r}_j$ reduces to a single term $\mathbf{r}$ for this electron. With some elementary calculations, the resulting cross section is